

Effect of Co, Ni, and Cu substitution on the electronic structure of hexagonal YMnO₃ studied by x-ray absorption spectroscopy

K. Asokan, Y. S. Chen, C. W. Pao, H. M. Tsai, C. W. O. Lee, C. H. Lin, H. C. Hsueh, D. C. Ling, W. F. Pong, J. W. Chiou, M.-H. Tsai, O. Peña, and C. Moure

Citation: [Applied Physics Letters](#) **95**, 131901 (2009); doi: 10.1063/1.3224905

View online: <http://dx.doi.org/10.1063/1.3224905>

View Table of Contents: <http://scitation.aip.org/content/aip/journal/apl/95/13?ver=pdfcov>

Published by the [AIP Publishing](#)

Articles you may be interested in

[Effect of spin frustration and spin-orbit coupling on the ferroelectric polarization in multiferroic YMnO₃](#)
Appl. Phys. Lett. **94**, 224107 (2009); 10.1063/1.3151912

[X-ray absorption and magnetic circular dichroism characterization of a novel ferromagnetic Mn_x phase in Mn / Si₃N₄ multilayers](#)
Appl. Phys. Lett. **93**, 252506 (2008); 10.1063/1.3050534

[Er coordination in Y₂O₃ thin films studied by extended x-ray absorption fine structure](#)
J. Appl. Phys. **100**, 023115 (2006); 10.1063/1.2214299

[The structural and electronic properties of nanostructured Ce_{1-x-y}Zr_xTb_yO₂ ternary oxides: Unusual concentration of Tb³⁺ and metal oxygen metal interactions](#)
J. Chem. Phys. **122**, 154711 (2005); 10.1063/1.1883631

[Soft x-ray absorption spectroscopy studies of \(110\) YBa₂Cu₃O_{6.9} thin film](#)
J. Appl. Phys. **93**, 2834 (2003); 10.1063/1.1544072

The logo for AIP Chaos is displayed on a red background with a geometric, low-poly pattern. The letters 'AIP' are in a large, white, sans-serif font, followed by a vertical bar and the word 'Chaos' in a smaller, white, sans-serif font.

CALL FOR APPLICANTS
Seeking new Editor-in-Chief

Effect of Co, Ni, and Cu substitution on the electronic structure of hexagonal YMnO_3 studied by x-ray absorption spectroscopy

K. Asokan,^{1,a)} Y. S. Chen,¹ C. W. Pao,¹ H. M. Tsai,¹ C. W. O. Lee,¹ C. H. Lin,¹ H. C. Hsueh,¹ D. C. Ling,¹ W. F. Pong,^{1,b)} J. W. Chiou,² M.-H. Tsai,³ O. Peña,⁴ and C. Moure⁵

¹Department of Physics, Tamkang University, Tamsui 251, Taiwan

²Department of Applied Physics, National University of Kaohsiung, Kaohsiung 811, Taiwan

³Department of Physics, National Sun Yat-Sen University, Kaohsiung 804, Taiwan

⁴Sciences Chimiques de Rennes, UMR 6226, Université de Rennes 1, Rennes, France

⁵Department of Electroceramics, Instituto de Cerámica y Vidrio, CSIC 28500, Madrid, Spain

(Received 22 July 2009; accepted 16 August 2009; published online 28 September 2009)

X-ray absorption spectroscopy measurements have been performed to elucidate local electronic and atomic structures of orthorhombic 3d-transition metal-doped yttrium manganites (YMnO_3) with chemical formulae $\text{YMn}_{2/3}\text{Me}_{1/3}\text{O}_3$ (Me=Co, Ni, and Cu). The Mn L_3 - and K -edges x-ray absorption near-edge structure (XANES) demonstrate the direct substitution of Me^{2+} for Mn^{3+} , so that the positive effective charge of Mn ions are increased. Me-doping is also found to induce substantial broadening of the Mn L_3 -edge feature, which suggests enhancement of the delocalization of Mn 3d e_g subbands and conductivity. Local spin density approximation (LSDA)+U (Hubbard U parameter) calculations were used to understand their electronic structures. © 2009 American Institute of Physics. [doi:10.1063/1.3224905]

Manganites have diverse unique properties, such as colossal magnetoresistance, metal-insulator transition, charge ordering, and multiferroic nature.¹⁻³ Most theoretical and experimental investigations have focused extensively on rare-earth (R)-based manganites with a general formula of RMnO_3 .⁴ Lanthanides with smaller ionic radii such as Er or Yb, crystallize to form a hexagonal structure, and so does Y. These hexagonal manganites are of a class of materials known as “Multiferroic materials,” which exhibit coexistence of magnetic and ferroelectric (FE) ordering. These materials have great potential for technological applications.³ Therefore, intensive effort has been made to understand the intrinsic properties of these multiferroic manganites.⁵ The mixed oxides with a general formula of $\text{YMn}_{1-x}\text{Me}_x\text{O}_3$ (Me=Co, Ni, and Cu) are of technological interest because of their negative temperature coefficient and the tunability of their magnetoelectric coupling.^{6,7} Recently, the electronic structure of YMnO_3 has been extensively studied both theoretically and experimentally.^{8,9} YMnO_3 is a FE, antiferromagnetic compound with a very low electrical conductivity. Upon doping with Me, it exhibits semiconducting behavior and good electrical conductivity.^{6,7} In this study, Me ions are doped in hexagonal YMnO_3 with a specific composition of $\sim 1/3$. This composition is known to exhibit diverse unusual properties in manganites and it is within the solubility limits in most of these compounds.^{6,7} The electronic and atomic structures of orthorhombic $\text{YMn}_{2/3}\text{Me}_{1/3}\text{O}_3$ (hereafter Me- YMnO_3) were investigated using x-ray absorption near-edge structure (XANES) and extended x-ray absorption fine structure (EXAFS) spectroscopy. XANES at the O K -edge reflects the density of unoccupied states, which can be compared with partial density of states (DOSs) obtained by first-

principles calculations to understand XANES spectra.¹⁰

The XANES and EXAFS measurements were carried out at the National Synchrotron Radiation Research Center in Hsinchu, Taiwan. The manganites in this work were synthesized by a standard solid state reaction. X-ray diffraction (XRD) and magnetization measurements of Me- YMnO_3 and YMnO_3 revealed that doping YMnO_3 with Me ions causes a structural change from hexagonal to an orthorhombic perovskite structure and a significant change in the magnetic properties.^{6,7}

Figure 1(a) presents the Fourier transform (FT) of the Mn K -edge EXAFS $k^3\chi$ spectra of Me- YMnO_3 and YMnO_3 shown as solid lines. The Mn K -edge FT spectra of Me- YMnO_3 samples differ clearly from that of YMnO_3 . In

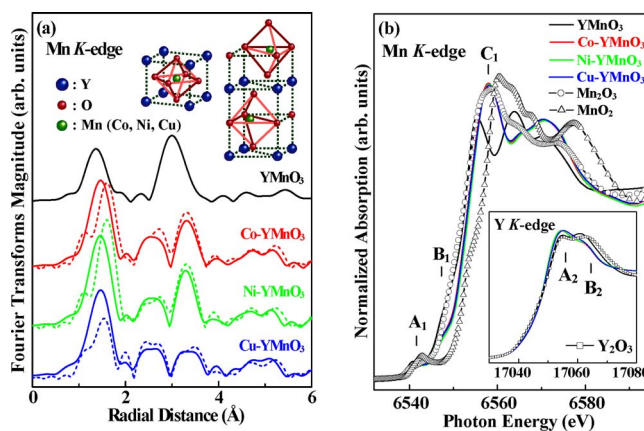


FIG. 1. (Color online) (a) FT spectra of Me- YMnO_3 (Me=Co, Ni, and Cu) and YMnO_3 . The dashed lines in EXAFS of Me- YMnO_3 at Co, Ni, and Cu K -edge are similar to the EXAFS FT spectra of Mn K -edge (solid lines). Inset in the top (i) perovskite structure (left-side) and (ii) hexagonal manganites (right side). (b) Normalized XANES spectra at Mn K -edge of Me- YMnO_3 and YMnO_3 along with the reference compounds MnO_2 and Mn_2O_3 . Inset presents the normalized XANES spectra at Y K -edge of Me- YMnO_3 , YMnO_3 , and Y_2O_3 .

^{a)}Permanent address: Inter-University Accelerator Centre, New Delhi-67, India.

^{b)}Electronic mail: wfpong@mail.tku.edu.tw.

YMnO₃, the local atomic structure of the Mn site is characterized by the presence of the MnO₅ bipyramid [right-hand inset, Fig. 1(a)] and in Me–YMnO₃, it is characterized by the MnO₆ octahedron [left-hand inset, Fig. 1(a)]. The FT spectral features of the nearest-neighbor Mn–O distance and the higher-neighbor shells also show the structural difference. The position and width of the first feature are related to the average Mn–O bond distance and its distribution, respectively. The Co, Ni, and Cu *K*-edge FT spectra overall are similar to the corresponding Mn *K*-edge FT spectra of Me–YMnO₃ samples (which are superimposed as dashed lines), except for the first main feature in the FT curves, which shifts toward larger radial distance from those of the Mn *K*-edge. This shift reflects the larger ionic radii of Co, Ni, and Cu cations than that of the Mn cation. The first main feature between 1 and 2 Å corresponds to the Mn–O (Me–O, in the case of dashed lines) bond distance. The second (~2.5 Å) and third (~3.3 Å) features correspond to Mn(Me)-Y and Mn(Me)-Me(Mn) bond distances in Me–YMnO₃,¹¹ respectively. The heights of the first main feature in the Cu *K*-edge FT curves of Cu–YMnO₃ are significantly reduced, which was argued to be due to the Jahn-Teller (JT) distortion caused by Cu cations.⁶ These EXAFS results suggest that Me ions substituted at Mn ions, which is consistent with XRD results.

The local electronic structures at the Mn site as observed in the normalized XANES spectra at the Mn *K*-edge of the samples are presented in Fig. 1(b) along with the reference compounds Mn₂O₃ and MnO₂. The pre-edge region is broad for Me–YMnO₃ and is similar to those observed for Ca- and Ce-doped LaMnO₃,^{12,13} but is different from that of YMnO₃. The pre-edge features **A**₁ to **B**₁ below the main feature **C**₁ are due to Mn 1*s* transition into unoccupied O 2*p*-Mn 3*d* (or Mn 3*d*/4*p*) hybridized states, which have *p* components projected at the Mn site as observed in many transition-metal oxides. The main feature **C**₁ at the Mn *K*-edge corresponds to the high-energy Mn 4*p* states. Figure 1(b) shows that the threshold of the first main Mn *K*-edge feature of YMnO₃ nearly coincides with that of Mn₂O₃, for which the Mn ion has been assigned to have a valence or effective charge of +3. The thresholds of the main Mn *K*-edge features of Me–YMnO₃ have higher energies than that of YMnO₃/Mn₂O₃, but have lower energies than that of MnO₂, for which the Mn ion has been assigned to have a valence of +4. The positions of the threshold energies of the main Mn *K*-edge features of Me–YMnO₃ seem to suggest that the Mn ions in Me–YMnO₃ have an (average) effective charge between +3 and +4. Thus, the doping of Me in YMnO₃ increases the positive effective charge of Mn ions. Other XANES for Me–YMnO₃ at the Co, Ni, and Cu *K*-edge (not shown here) were similar to corresponding divalent state oxides. The inset in Fig. 1(b) presents the XANES spectra at the Y *K*-edge of Me–YMnO₃, YMnO₃, and Y₂O₃. The Y ion in YMnO₃ is monocoordinated and octahedrally coordinated. YMnO₃ and Y₂O₃ yield similar spectral line shapes with a twin-peak features (**A**₂ and **B**₂) separated by ~6 and 7 eV, respectively, suggesting that the Y ions in both compounds are in similar environments.¹⁴ However, the threshold position of feature **A**₂ for Me–YMnO₃ did not shift with respect to those for YMnO₃ and Y₂O₃, indicating that the effective charge of Y ions in Me–YMnO₃ is similar to those in YMnO₃ and Y₂O₃.

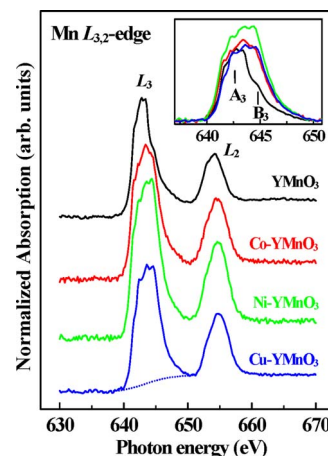


FIG. 2. (Color online) (a) Normalized Mn *L*_{3,2}-edge XANES spectra of Me–YMnO₃ and YMnO₃. Inset presents a magnified view of the near-edge features, **A**₃ and **B**₃, at the Mn *L*₃-edge after the background has been subtracted using a step function, indicated by the dotted line.

Figure 2 displays the normalized Mn *L*_{3,2}-edge XANES spectra of Me–YMnO₃ and YMnO₃. These spectra are primarily associated with the Mn 2*p* → 3*d* transition, and the intensity of the white line can be regarded as a measure of the density of unoccupied Mn 3*d* states. The inset in Fig. 2 presents a magnified view of the near-edge features, **A**₃ and **B**₃, at the Mn *L*₃-edge after the background has been subtracted. As revealed in the inset of the figure, the centroid shifts upward in energy with the doping of Me ions and the integrated area under the feature exceeds that of YMnO₃. This result shows an increase in the number of unoccupied Mn 3*d* states, reflecting a decrease in the 3*d*-states occupation and an increase in the positive effective charge of Mn ions consistent with the argument given previously for the shift of the threshold position of the main Mn *K*-edge feature to higher energy relative to that of YMnO₃. The Me-doping induced increase in the effective charge of Mn ions indicated the direct substitution of Me²⁺ for Mn³⁺, to preserve the valence equilibrium in Me–YMnO₃. Figure 2 also shows that the overall Mn *L*₃-edge features for Me–YMnO₃ are greatly broadened relative to that of YMnO₃, which reveals that the doping of Me ions promoted delocalization of Mn 3*d* states and the improvement of conductivity as observed.^{6,7} The inset in Fig. 2 presents the intensity changes of features **A**₃ and **B**₃ in the spectra of Me–YMnO₃ relative to that of YMnO₃. Features **A**₃ and **B**₃ are typically assigned to the Mn 3*d* *t*_{2*g*} and *e*_g bands, respectively. However, the spin-polarized partial DOSs obtained from local spin density approximation (LSDA)+U (Hubbard *U* parameter) calculations for Me–YMnO₃ revealed that features **A**₃ and **B**₃ are primarily associated with the Mn majority-spin (indicated as ↑-spin) *e*_g and minority-spin (↓-spin) *t*_{2*g*}/*e*_g subbands,¹⁰ respectively.

Figure 3(a) displays the normalized XANES spectra of Me–YMnO₃ at the O *K*-edge. For comparison, the lower inset presents the spectrum of YMnO₃. Four major features in the spectra, labeled as **A**₄–**D**₄, are centered at ~529, 531, 535, and 540 eV, respectively. These features provide detailed information about the unoccupied O 2*p*-derived states commonly observed in perovskite oxides. Features **A**₄ and **B**₄ vary remarkably in the spectra of the three Me–YMnO₃ compounds, which are magnified in the upper inset of Fig. 3(a), after the background has been subtracted. They are

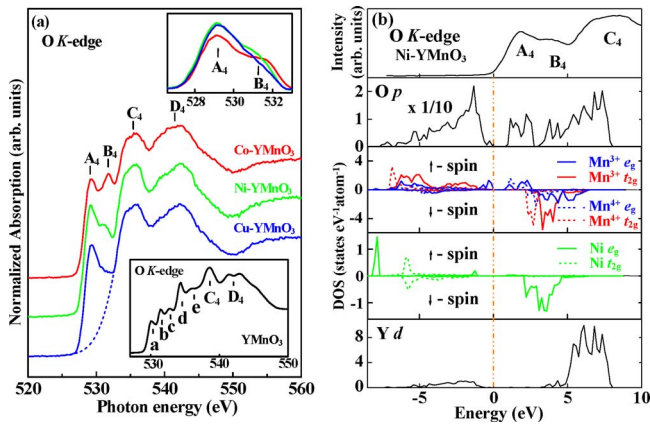


FIG. 3. (Color online) (a) O K -edge XANES spectra of the three Me–YMnO₃ compounds. The lower inset presents normalized XANES spectra at the O K -edge of YMnO₃ (Ref. 8). The upper inset presents a magnified view of near-edge features at the O K -edge after the background has been subtracted using a best-fitted Gaussian curve, indicated by the dotted line. (b) Comparison of the O K -edge XANES features of Ni–YMnO₃ (upper solid line) with the theoretical spin-polarized partial DOSs of YMn_{0.75}Ni_{0.25}O₃. The spectra have been aligned with the first peak and the Fermi level is defined as the zero energy.

conventionally assigned to TM $3d$ -O $2p$ hybridized states. Spin-polarized electronic structure of Ni–YMnO₃ has been obtained by Ou Lee *et al.*¹⁰ using the Vienna *Ab-initio* Simulation Package with LSDA+U.¹⁵ An efficient projector augmented-wave potential is used to describe the electron-ion interactions.¹⁶ Y($4s4p5s4d$), Mn($4s3d$), Ni($4s3d$), and O($2s2p$) are treated as valence electrons. The integration over the first Brillouin zone of the orthorhombic structure is approximated by sampling a $4 \times 4 \times 2$ k -point mesh. A kinetic energy cutoff of 450 eV is chosen for the plane wave basis set. In order to get reasonable value of band gap and magnetic properties of Ni–YMnO₃, the on-site Coulomb interaction $U=8$ eV and Hund's rule exchange interaction $J=0.88$ eV are selected for Mn $3d$ orbitals.¹⁷ Figure 3(b) compares the O K -edge XANES spectrum with calculated spin-polarized partial DOSs of Ni–YMnO₃. Due to the limitation of the unit cell, a concentration of 0.25 of Ni is considered, which is close to the experimental value of 1/3. It is observed that at temperature above the paramagnetic insulator-ferromagnetic metal transition, the spectrum is composed of the only one peak, while in the ferromagnetic region it splits into doublet due to the transition into e_g \uparrow -spin and t_{2g} \downarrow -spin states.¹⁸ These spectral features were observable in Me-doped YMnO₃. Consistent to this Ni- and Co–YMnO₃ are ferromagnets with a weak antiferromagnetic component and thus exhibit spectral feature **B**₄. However, because of the strong JT Cu²⁺ ion in Cu–YMnO₃, the spectral feature **B**₄ is very weak implying the characteristic of antiferromagnetic (or spin-glass) ordering. Figure 3(b) suggests that feature **A**₄ is contributed by O $2p$ and Mn $3d$ \uparrow -spin e_g hybridized states, while feature **B**₄ is contributed not only by O $2p$ and Mn $3d$ \downarrow -spin t_{2g} hybridization for both Mn³⁺ and Mn⁴⁺ valence states but also by Ni $3d$ \downarrow -spin e_g states, which have p components projected on the O sites. Feature **C**₄ corresponds to O $2p$ and Y $4d$ hybridized states and feature **D**₄ corresponds to Mn/Ni $4sp/Y$ $5sp$ states (not shown in the figure). This assignment is generally applicable to other cations such as Co and Cu ions. The changes in the intensities of features **A**₄ and **B**₄ in the spectra of

Me–YMnO₃ are primarily due to changes in the hybridization between O $2p$ orbitals and the Mn $3d$ \uparrow -spin e_g subband and Me $3d$ \downarrow -spin e_g subband, respectively.^{13,18} The intensities of features **A**₄ and **B**₄ shown in the upper inset of Fig. 3(a) for the three Me ions vary remarkably, indicating that occupation of Me $3d$ orbitals, which determines physical properties such as magnetic interactions, is important. Inset (lower) in Fig. 3(a) shows the XANES at O K -edge of YMnO₃ and spectral assignments given in Ref. 8.

Since Me–YMnO₃ has a similar perovskite structure as Ba (or Ca and Sr) doped LaMnO₃, its electric property may be understood by analogy with that of doped LaMnO₃. When some La ions are substituted by Ba (or Ca and Sr) ions in LaMnO₃, it has been commonly argued that a corresponding number of Mn³⁺ ions become Mn⁴⁺ ions. Similar change occurs by Co and Ni ions doping in orthorhombic LaMnO₃.^{19,20} The double exchange theory argued that the hopping of itinerant e_g electrons between spin-aligned Mn³⁺ and Mn⁴⁺ ions leads to a double-exchange interaction that results in enhancement of the conductivity.² Furthermore, O K -edge XANES spectra and theoretical calculations also consistently demonstrate the major difference of feature **B**₄, which corresponds to the Ni $3d$ \downarrow -spin e_g subband, further suggesting that Ni $3d_{x^2-y^2}$ -O $2p$ orbitals overlap in the basal plane to form a narrow $\sigma_{x^2-y^2}^*$ band of highly correlated itinerant electronic states, while the Ni $3d_{z^2}$ orbitals are more localized. Me doping in these Me–YMnO₃ improves the conductivity and eventually change the structural and magnetic properties.

¹A. J. Millis, *Nature (London)* **392**, 147 (1998).

²M. B. Salamon and M. Jaime, *Rev. Mod. Phys.* **73**, 583 (2001).

³T. Kimura, T. Goto, H. Shintani, K. Ishizaka, T. Arima, and Y. Tokura, *Nature (London)* **426**, 55 (2003).

⁴J. M. D. Coey, M. Viret, and S. von Molnar, *Adv. Phys.* **48**, 167 (1999).

⁵S. W. Cheong and M. Mostovoy, *Nature Mater.* **6**, 13 (2007).

⁶C. Moure, D. Gutierrez, O. Peña, and P. Duran, *J. Solid State Chem.* **163**, 377 (2002).

⁷D. Gutierrez, O. Peña, P. Duran, and C. Moure, *J. Eur. Ceram. Soc.* **22**, 567 (2002).

⁸K. Asokan, C. L. Dong, C. W. Bao, H. M. Tsai, J. W. Chiou, C. L. Chang, W. F. Pong, P. Duran, C. Moure, and O. Peña, *Solid State Commun.* **134**, 821 (2005).

⁹D. Y. Cho, J. Y. Kim, B. G. Park, K. J. Rho, J. H. Park, H. J. Noh, B. J. Kim, S. J. Oh, H. M. Park, J. S. Ahn, H. Ishibashi, S. W. Cheong, J. H. Lee, P. Murugavel, T. W. Noh, A. Tanaka, and T. Jo, *Phys. Rev. Lett.* **98**, 217601 (2007).

¹⁰C. W. Ou Lee, C. H. Lin, and H. C. Hsueh (unpublished).

¹¹M. C. Sánchez, G. Subías, J. García, and J. Blasco, *Phys. Rev. Lett.* **90**, 045503 (2003).

¹²F. Bridges, C. H. Booth, G. H. Kwei, J. J. Neumeier, and G. A. Sawatzky, *Phys. Rev. B* **61**, R9237 (2000).

¹³K. Asokan, J. C. Jan, K. V. R. Rao, J. W. Chiou, H. M. Tsai, S. Mookerjee, W. F. Pong, M.-H. Tsa, R. Kumar, S. Husain, and J. P. Srivastava, *J. Phys.: Condens. Matter* **16**, 3791 (2004).

¹⁴M. Malvestuto, R. Carboni, F. Boscherini, F. Boscherini, F. D'Acapito, S. Spiga, M. Fanciulli, A. Dimoulas, G. Vellianitis, and G. Mavrou, *Phys. Rev. B* **71**, 075318 (2005).

¹⁵G. Kresse and J. Hafner, *Phys. Rev. B* **49**, 14251 (1994).

¹⁶P. E. Blöchl, *Phys. Rev. B* **50**, 17953 (1994).

¹⁷S. Satpathy, Z. S. Popovic, and F. R. Vukajlovic, *Phys. Rev. Lett.* **76**, 960 (1996).

¹⁸E. Pellegrin, L. H. Tjeng, F. M. F. de Groot, R. Hesper, G. A. Sawatzky, Y. Moritomo, and Y. Tokura, *J. Electron Spectrosc. Relat. Phenom.* **86**, 115 (1997).

¹⁹J.-H. Park, S. W. Cheong, and C. T. Chen, *Phys. Rev. B* **55**, 11072 (1997).

²⁰M. C. Sánchez, J. García, J. Blasco, G. Subías, and J. Perez-Cacho, *Phys. Rev. B* **65**, 144409 (2002).